ADVANCED FUNCTIONAL MATERIALS
www.afm-journal.de

Unusual Circularly Polarized Photocatalytic Activity in Nanogapped Gold–Silver Chiroplasmonic Nanostructures

Changlong Hao, Liguang Xu, Wei Ma, Xiaoling Wu, Libing Wang, Hua Kuang, and Chuanlai Xu*

Gold-gap-silver nanostructures (GGS NSs) with interior nanobridged gaps are enantioselectively fabricated. Guided by L/D-cysteine, the GGS-L/D (L/D represents L/D-cysteine) NSs show reversed plasmon-induced circular dichroism (CD) signals in the visible region. It is found that the nanogap plays a key role in the plasmonic CD of GGS NSs and the chiroptical response can be tailored by adjusting the amount of cysteine. The anisotropy factor of GGS-L/D NSs with a 0.5 nm interior gap at 430 nm is as high as ≈0.01. The circularly polarized photocatalytic activity of GGS NSs is examined. It is shown that upon irradiation with left-circularly polarized light, the catalytic efficiency of GGS-L NSs is 73-fold and 17-fold higher than that of Au nanoparticles (NPs) and Au@Ag core–shell NPs, respectively. Upon irradiation with right-circularly polarized light, the catalytic activity of GGS-D NSs is about 71 times and 17 times higher than that of Au NPs and Au@Ag core–shell NPs, respectively. These unique chiral NSs with high plasmonic response can be applied to enantioselective catalysis.

1. Introduction

Over the past decade, considerable attention[1–7] has been paid to the chirality of microscale[8] and nanoscale inorganic structures due to their wide application including chiral sensing,[9–12] enantioselective recognition and separation,[13,14] optical devices, and other aspects.[15,16] Many inorganic chiral nanostructures (NSs) with controlled composition and morphology have been prepared. However, most reports on the preparation of chiral plasmonic architectures have focused on assembling achiral building blocks and chiral molecules into 2D and 3D structures[17–33] (film,[18,25] tetramer,[22] pyramid,[24,26,34] helix[27–32] or generating a relatively weak chiroptical response through the interaction between chiral organic ligands and achiral metals (AuNP[35–37] or AgNP[38,39]) or semiconductor nanocrystals (CdS,[40] CdSe,[41] or CdTe[42]).

Dr. C. Hao, Dr. L. Xu, Dr. W. Ma, Dr. X. Wu, Prof. L. Wang, Prof. H. Kuang, Prof. C. Xu
State Key Lab of Food Science & Technology
School of Food Science & Technology
Jiangnan University
Wuxi 214122, China
E-mail: kuangh@jiangnan.edu.cn

DOI: 10.1002/adfm.201502429

There have been some reports on the synthesis of intrinsically chiral inorganic nanoparticles (NPs) with intense optical activity. Markovich and colleagues[43] reported the synthesis of α-HgS (cinnabar) NPs with lattice chirality. Govorov and colleagues[44] synthesized Te and Se NSs with lattice and shape chirality. More recently, our group[45] reported the preparation of a gold core-DNA-silver shell NPs with strong plasmonic chiroptical activity, where the CD signal could only be adjusted in the positive part, and only one enantiomer of a Au core-DNA-Ag shell NPs was obtained. Moreover, the synthesis of core–shell gold-gap-gold NSs (GGG NSs) using DNA[46–48] or amphiphilic block copolymers[49] has been achieved. However, the gap size of GGG NSs synthesized with DNA cannot be tailored, and the process of GGG NSs prepared with polymer is very complex.

Because of the synergistic effect, bimetallic NPs including core–shell Au@Ag NPs display superior catalytic performance than their single counterparts.[50] Although there are many reports about the preparation of Au@Ag NPs,[45,50–52] the synthesis of gold-gap-silver NSs (GGS NSs) with tailorable nanogaps has never been reported. Here, we report the synthesis of a new class of GGS-L/D (L/D represents L/D-cysteine) NSs, which display strong and reversed chiroptical activity in the Ag plasmonic region.

Circularly polarized light (CPL), a chiral form of light, has attracted considerable attention, which was used as the chiral source to initiate photochemical reactions and trigger changes in chiral systems.[53–57] For example, CPL was used to assemble racemic CdTe NPs into twisted nanoribbons with an enantiomeric excess exceeding 30%.[19] CPL was also employed to assemble a triphenylamine moiety into helical NSs with supermolecular chirality[55] and to form chiral polydiacetylene films.[58] In addition, high-intensity CPL irradiation led to the dynamic control and amplification of molecular chirality.[54]

Significantly, in the present work, unexpected circularly polarized photocatalytic activity is discovered based on the fabricated GGS NSs under the irradiation of CPL. To the best of our knowledge, this is the first example that CPL is combined with intrinsically chiroplasmonic GGS NSs to greatly increase the catalytic reaction rate.

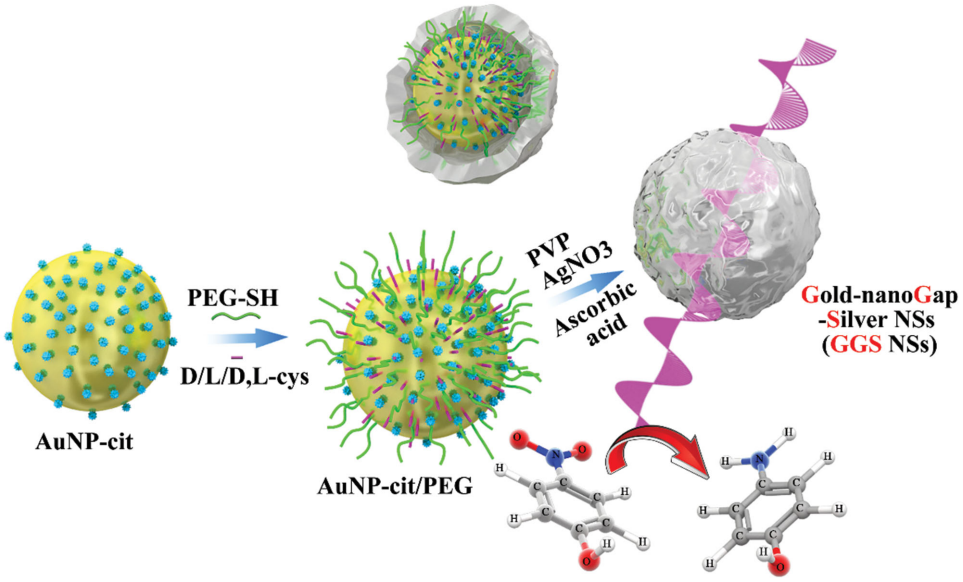

Figure 1. Schematic illustration of the preparation of chiral GGS NSs.

2. Result and Discussion

As illustrated in **Figure 1**, the GGS NSs were synthesized from citrate-capped Au NPs (AuNP-cit, 15 ± 2 nm in diameter). In the typical synthesis of GGS-L-0.01 NSs (L-0.01 represents 0.01×10^{-3} M L-cys), first, via gold-thiolcovalant bonding, methoxy-polyethylene glycol-thiol (PEG-SH) and 0.01×10^{-3} M of L-cys were modified on the surface of AuNP-cit to form AuNP-L-cys/PEG, which was then used as seeds for GGS-L NSs. PEG-SH was used to prevent the formation of disordered AuNP aggregates initiated by the cysteine molecules. After 0.5 h incubation, AuNP-L-cys/PEG was isolated by centrifugation. Subsequently, stabilizer (polyvinylpyrrolidone, PVP), reductant (L-ascorbic acid), and precursor ($AgNO_3$) were added sequentially to form the GGS-L-0.01 NSs. A similar strategy was used for the synthesis of other GGS NSs such as GGS-L-0.05 and GGS-D-0.01 NSs. See the Supporting Information for more details.

Transmission electron microscopy (TEM) image analysis of intermediate structures, UV–vis, and CD spectroscopy were performed for a better understanding of the synthetic process of the GGS NSs. The typical dynamic growth process of GGS-L-0.01 NSs is presented in **Figure 2**A–F. In the initial stage, the Au–Ag heterodimer (intermediate at 5 min, Figure 2B) was formed by growth of the budding Ag structure on the Au core surface. From 5 to 20 min (Figure 2B–E), further growth and interconnection of the budding NSs resulted in a complete Ag shell and interior nanogaps. Importantly, TEM images (Figure 2E,F) confirmed that the nanobridges which connected the Au core and the outer Ag shell were formed. For GGS-D-0.01 NSs (D-0.01 represents 0.01×10^{-3} M D-cys), dynamic TEM images shown in Figure S1 (Supporting Information) were silmilar to GGS-L-0.01 NSs.

The dynamic UV–vis results are shown in Figure S2 (Supporting Information), which were well-matched with the structural changes demonstrated by TEM images. The spectrum for the Au–Ag heterodimer showed two bands: Ag transverse plasmonic absorbance band at around 410 nm, and the Au–Ag longitudinal plasmonic peak at 580 nm and this band was changed by different Ag islands. As the complete Ag shell grows (from 5 to 20 min), this longitudinal band gradually shifts to shorter wavelengths (blueshift) and disappears. Simultaneously, the Ag surface plasmon resonance (SPR) band gradually shifts to longer wavelengths (redshift) and the peak intensity gradually increases. The final product only showed one band at 430 nm without the longitudinal plasmonic absorbance.

Notably, the dynamic growth process of GGS NSs provides an opportunity to explore the relationship between chiroptical activity and the conformation of chiral plasmonic NS. The dynamic CD spectra of GGS-L-0.01 and GGS-D-0.01 NSs as a function of reaction time are shown in Figure 2G. In the region from 350 to 700 nm, for GGS-L-0.01 NS, the CD spectrum for the Au–Ag heterodimer NS (Figure 2G, red line) showed three new peaks. The CD peak at around 580 nm can be attributed to the longitudinal SPR of the Au–Ag heterodimer. The other two peaks at 360 and 405 nm exhibited a Cotton effect, which is assigned to the Ag transverse plasmonic resonance. As expected, the changes in CD spectra were in accordance with the UV–vis spectra. Synchronous with the formation of the Ag shell, a gradual increase in chiroptical activity was observed in the Ag plasmonic part of the CD spectra. From 5 to 20 min, the Ag plasmonic CD (PCD) peak was gradually redshifted from 405 to 425 nm, and the CD intensity was increased from 23 ± 1.2 mdeg to 62 ± 3.1 mdeg. With regard to the Au PCD peak from 5 to 10 min, it was shifted from 570 to 535 nm and the intensity decreased from 6.2 ± 0.4 mdeg to 2.5 ± 0.1 mdeg. The Au PCD peak disappeared at 15 min and there was no Au SPR peak in the UV–vis spectrum. Note that GGS-L-0.01 and GGS-D-0.01 NSs exhibited identical optical absorbance features in the range 200–700 nm spectra window (Figure S2, Supporting Information), but displayed opposite line shapes in CD spectra in the same region (Figure 2G), indicating the generation of opposite crystal enantiomers.

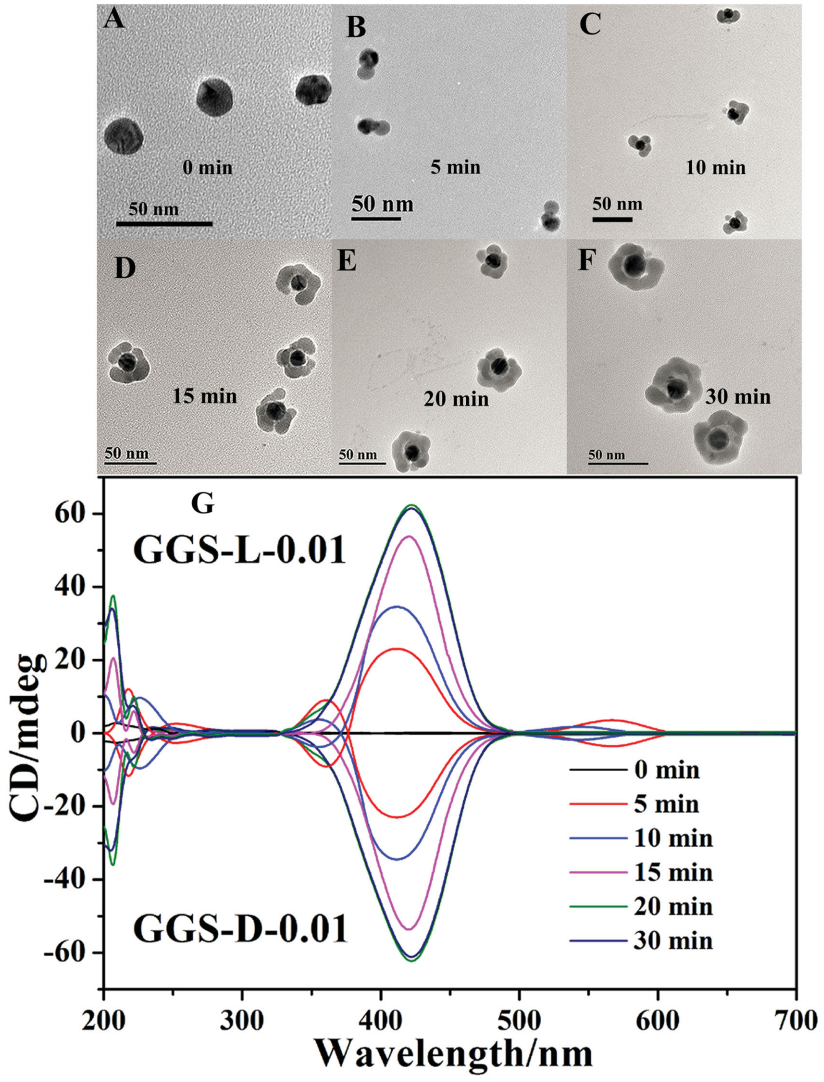

Figure 2. A–F) Representative TEM images of GGS-L-0.01 NSs for different reaction times. G) Dynamic CD spectra of GGS-L-0.01 NSs and GGS-D-0.01 NSs. Note: The Arabic number represents the concentration of cysteine, for example, "L-0.01" stands for a L-cys concentration of 0.01×10^{-3} M, "D-0.01" stands for a D-cys concentration of 0.01×10^{-3} M.

The formation of GGS NSs with interior nanogaps was significant for the intensity of the CD signal. Therefore, the relationship between the size of the interior gap and the CD signal was explored. The nanogap size of GGS NSs was manipulated by changing the amount of L-/D-/D,L-cys (**Figure 3**). When the concentration of L-/D-/D,L-cys was 0.01×10^{-3} M, the nanogap sizes in the GGS-L/D/D,L-0.01 NSs were 0.5 ± 0.1, 0.5 ± 0.2, and 0.4 ± 0.2 nm (Figure 3A–C). When the concentration of L-/D-cys increased to 0.05×10^{-3} M, the nanogap sizes in the GGS-L/D-0.05 NSs were expanded to 1.1 ± 0.5 and 1.2 ± 0.4 nm, respectively (Figure 3D,E). When no cysteine was used in the synthetic process, core–shell Au@Ag NPs without nanogaps were formed (Figure 3F). In the case of 0.1×10^{-3} M L-cys, NSs with large multinanohole-like gaps were formed (Figure S8, Supporting Information), and the GGS-L-0.1 NSs were unstable and aggregated with increasing time. In subsequent experiments, 0.01×10^{-3} and 0.05×10^{-3} M D/L-cys were chosen for the fabrication of GGS NSs.

Optical properties of the GGS NSs and the control samples were characterized by CD and UV–vis spectroscopy. The UV–vis spectra of the GGS NSs were almost superposition to each other as shown in Figure S9 (Supporting Information), while the core–shell Au@Ag NPs showed a relatively narrow peak in the same region as GGS NSs.

As shown in Figure 3G, the CD spectra of GGS NSs displayed a good mirror image by choosing the opposite enantiomer of cysteine. In the UV region, GGS-L-0.01/0.05 and GGS-D-0.01/0.05 NSs exhibited CD signals at 200–250 nm, which were due to the chiral cysteines in the GGS NSs, and the intensity of the CD signals was much stronger than that of pure cysteine enantiomers in the solution. Furthermore, the CD signal intensity of GGS-L/D-0.01 NSs was nearly twice that of GGS-L/D-0.05 NSs.

In the visible region (400–700 nm), the PCD peak around 430 nm was assigned to the Ag SPR. Although less cysteine was used, the PCD signal intensity of GGS-L-0.01 NSs (500 ± 12 cysteine molecules per NS, see detailed analysis in the Supporting Information) was much higher than that of GGS-L-0.05 NSs (850 ± 41 cysteine molecules per NS). The stronger PCD intensity of GGS-L-0.01 NSs was attributed to the smaller nanogap size. Note that no CD signal was detected for GGS-D,L-0.01 NSs, which were prepared using 0.01×10^{-3} M D,L-cys. As shown in Figure S10 (Supporting Information), the maximum g-factor in GGS NSs was −0.010 for GGS-D-0.01 NS and +0.011 for GGS-L-0.01 NS, which was quite high for individual nanocrystals[43,44] and was comparable with assembled systems.[10,24,28,45] The control samples, PVP, PEG-SH, AuNP, Au@Ag, the individual AuNP modified with L-/D-/D,L-cys and PEG-SH (AuNP-L-cys/PEG, AuNP-D-cys/PEG, AuNP-D,L-cys/PEG) showed no PCD signals in the visible region.

Electron tomography analysis was performed to provide structural information on the GGS NSs and Au@Ag NPs. From the holistic perspective of the electron tomography image (**Figure 4**A,E), the surface of both Au@Ag NPs and GGS-L-0.01 NSs was uneven and bumpy; and from the cutaway view (Figure 4B,F), the nanogap can only be observed in the cross section of GGS NSs, which provides additional visual evidence of the nanogaps. Energy dispersive X-ray elemental mapping images (Figure 4D,H) showed the distinct compositional distribution of Au and Ag. Compared with Au@Ag NPs, GGS NSs displayed a particular area without elemental distribution, which corresponded to the nanogaps.

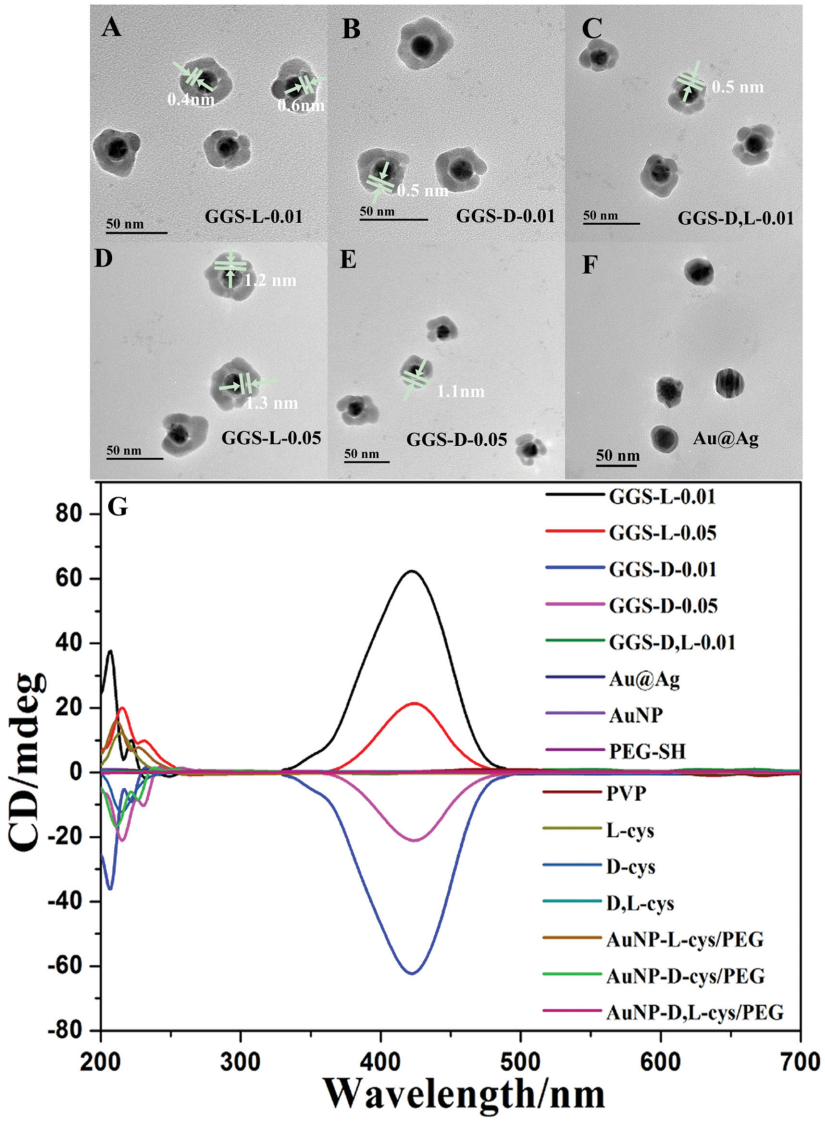

Figure 3. TEM images of A) GGS-L-0.01 NS, B) GGS-D-0.01 NS, C) GGS-D,L-0.01 NS, D) GGS-L-0.05 NS, E) GGS-D-0.05 NS, and F) Au@Ag NP. G) CD spectra of GGS-L-0.01 NS, GGS-L-0.05 NS, GGS-D-0.01 NS, GGS-D-0.05 NS, GGS-D,L-0.01 NS, Au@Ag, AuNP, PEG-SH, PVP, L-cys, D-cys, D,L-cys, AuNP-L-cys/PEG, AuNP-D-cys/PEG, and AuNP-D,L-cys/PEG. Note: The Arabic number represents the concentration of cysteine, for example, "L-0.01" stands for a L-cys concentration of 0.01×10^{-3} M, "D-0.01" stands for a D-cys concentration of 0.01×10^{-3} M.

High-resolution TEM (HRTEM) was also performed, and as shown in Figure 4C, the HRTEM image indicated that the Ag shell of Au@Ag NPs grew epitaxially on the AuNP surface, and the 0.23 nm lattice spacing belonged to the Ag (111) crystal plane, which was consistent with a previous report.[45] In comparison, the GGS-L-0.01 NSs showed a clear interior nanogap with a width of 1.1 nm and a polycrystalline structure with lattice spacing of 0.20 and 0.23 nm (Figure 4G).

The origin of the plasmonic CD response of GGS NSs synthesized by chiral D/L-cys was explored. The plasmonic chirality of GGS NSs may originate due to the following two aspects: (1) a chiral cysteine–plasmon dipolar interaction; (2) plasmonic hot-spot-induced CD amplification.[59] On the one hand, GGS NSs obtained using D,L-cys showed no CD signals (Figure 3G). Importantly, when no chiral molecules (D/L-cys) were added in the synthetic process, no detectable CD response was observed, which revealed the chiral cysteine–plasmon interaction induced PCD of GGS-D/L NSs. That is to say, the plasmonic CD comes from the chiral currents inside the metal nanocrystal induced by the dipole of the chiral molecule.[60] On the other hand, the GGS-L/D-0.01 NSs showed much higher CD signals than the GGS-L/D-0.05 NSs, which indicated that the latter made a dominant contribution to the PCD signal. As shown in the electromagnetic simulation results, the electric field intensity in the GGS NSs with a 0.5 nm gap was greater than that in the GGS NSs with a 1.1 nm gap which in turn was greater than that in the Au@Ag NPs without a nanogap (Figure S11, Supporting Information). This was due to the smaller gap size which caused higher electromagnetic enhancement at the plasmonic hot spots. Surface enhanced Raman scattering (SERS) spectra (Figure S12 and S13, Supporting Information) revealed that the GGS-L/D-0.01 NSs (0.5 nm gap) owned much higher SERS intensity compared with the GGS-L/D-0.05 NSs (1.1 nm gap), which was consistent with the calculated results. In addition, plasmon resonances of the GGS NSs resulted in the enhancement of the CD signals of chiral molecules (Figure 3G), which probably resulted from the plasmon-induced amplification in the electromagnetic field inside the chiral molecule.

A well-known model reaction (4-nitrophenol was reduced to 4-aminophenol in the presence of excess $NaBH_4$) was applied to evaluate the circularly polarized photocatalytic activity of the GGS-L-0.01 NSs. The 4-nitrophenol could not be reduced in the absence of catalysts. The reaction process was monitored through UV–vis absorption spectroscopy (Figure S17, Supporting Information). **Figure 5**A showed the logarithm plot of the absorbance with reaction time, the kinetic rate constant is estimated to be 0.73 min^{-1} for GGS-L-0.01 NSs (15 ± 2 nm Au core, 0.5 ± 0.1 nm gap, and 10 ± 1 nm Ag shell) irradiated by left-circularly polarized (LCP) light, which was about 5-fold, 10-fold, 11-fold, and 12-fold higher than those of the photocatalytic reactions irradiated by linearly polarized (LP) light (0.14 min^{-1}), right-circularly polarized (RCP) light (0.072 min^{-1}), natural light (0.065 min^{-1}), and without light (0.061 min^{-1}), respectively. The intensity of the different light sources is at the same levels of 1.5 W.

The catalytic performance of GGS-L-0.01 NSs with Au NPs, Ag NPs, Au@Ag NPs, and GGS-D-0.01 NSs under the identical conditions was compared (Figure S18, Supporting Information). As shown in Figure 5B, under the irradiation of LCP light, the kinetic rate constants of GGS-L-0.01 NSs were about

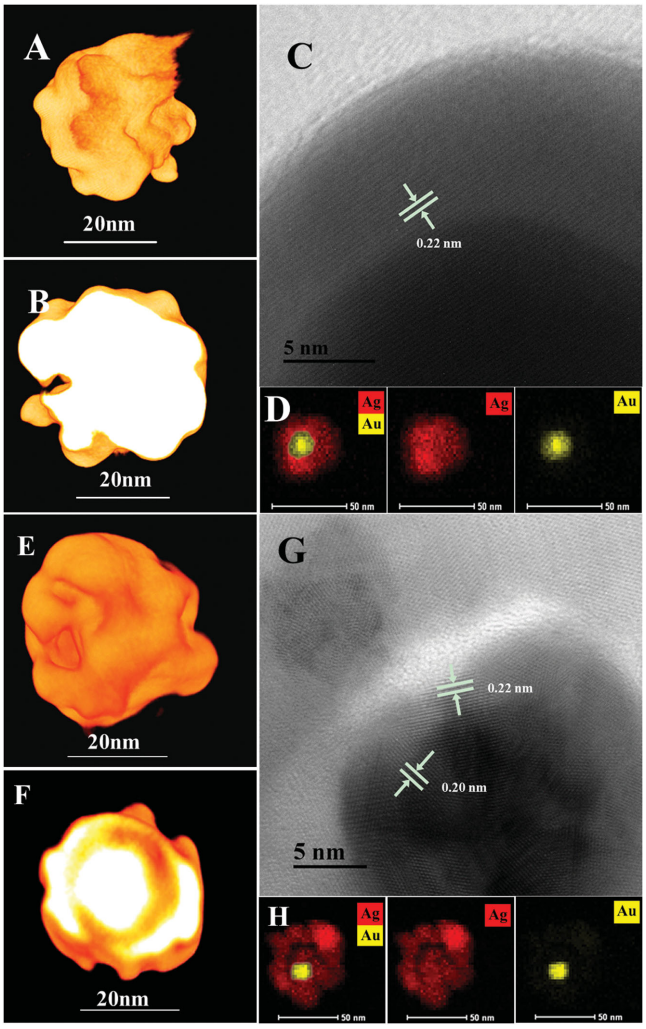

Figure 4. A) 3D electron tomography reconstructions of Au@Ag, B) cutaway view of the Au@Ag, C) HRTEM of Au@Ag, D) STEM-EDS elemental mapping images of Au@Ag, E) 3D electron tomography reconstructions of GGS-L-0.01, F) cutaway view of the GGS-L-0.01, G) HRTEM of GGS-L-0.01, and H) STEM-EDS elemental mapping images of GGS-L-0.01. Note: The Arabic number represents the concentration of cysteine, for example, "L-0.01" stands for a L-cys concentration of 0.01×10^{-3} M, "D-0.01" stands for a D-cys concentration of 0.01×10^{-3} M.

73-fold, 40-fold, 17-fold, and 16-fold higher than those of Au NPs (15 ± 2 nm, 0.010 min^{-1}), Ag NPs (15 ± 3 nm, 0.018 min^{-1}), Au@Ag NPs (15 ± 2 nm Au core and 10 ± 1 nm Ag shell thickness, 0.043 min^{-1}), and GGS-D-0.01 NSs (15 ± 2 nm Au core, 0.5 ± 0.2 nm gap, and 10 ± 1 nm Ag shell, 0.045 min^{-1}), respectively.

The reason why LCP light led to the highest catalytic efficiency was that LCP light activated a larger number of GGS-L-0.01 NSs than other light conditions, which increased the number of hot electron of chiral NSs by adsorbing the related rotation of polarized light.[61] Moreover, due to the strong synergistic effects of bimetallic NSs, GGS-L-0.01 NSs showed much higher catalytic activity than the corresponding monometallic NSs, which was consistent with previous studies.[50,52] As expected, for GGS-D-0.01 NSs, the RCP light triggered the highest catalytic activity (Figure 5C and Figure S19 in the Supporting Information) compared to other light conditions. The kinetic rate constant of GGS-D-0.01 NSs was 0.71 min^{-1}, which was about 5-fold, 10-fold, 11-fold, and 12-fold higher than those of the photocatalytic reaction irradiated by LP light (0.14 min^{-1}), LCP light (0.074 min^{-1}), natural light (0.062 min^{-1}), and without light (0.06 min^{-1}), respectively. Figure 5D and Figure S20 in the Supporting Information displayed that under the same RCP light irradiation, GGS-D-0.01 NSs were the most powerful catalysts, the kinetic rate constants were about 71-fold, 39-fold, 17-fold, and 16-fold higher than those of Au NPs (0.010 min^{-1}), Ag NPs (0.018 min^{-1}), Au@Ag NPs (0.042 min^{-1}), and GGS-L-0.01 NSs (0.044 min^{-1}), respectively. The results confirmed that the CPL could activate hot electrons of chiral NPs, which led to the much higher catalytic activity.

3. Conclusion

GGS-L/D NSs with distinctive plasmon-induced chiroptical performance in the visible region were shown for the first time, which represents great progress in the enantioselective fabrication of chiral plasmonic NSs with tailored optical chirality. The PCD activity could be tailored by altering the amount of chiral cysteine, which was also used to tailor the nanogap size of GGS NSs. The plasmonic chirality of GGS NSs was caused by the dipole interaction between chiral cysteine and plasmon coupling, and the electromagnetic coupling further enhanced the PCD response. The relationship between the size of interior gaps and the SERS signal was also illustrated. Importantly, the chiral GGS NSs showed unusual circularly polarized photocatalytic activity under CPL irradiation. It is expected that the synthetic principle described here can be applied to the enantioselective synthesis of high g-factor chiral NSs. Furthermore, the chiral GGS NSs open up avenues for chiral catalysis and biosensing.

4. Experimental Section

Materials: Trisodium citrate ($C_6H_5Na_3O_7 \cdot 2H_2O$, ≥99.0%), tetrachloroauric acid trihydrate ($HAuCl_4 \cdot 3H_2O$, 99.9%), poly(vinylpyrrolidone) (PVP; M_w = 10 000), L-cysteine (L-cys), D-cysteine (D-cys), D,L-cysteine (D,L-cys), 4-nitrophenol (4-NP), silver nitrate ($AgNO_3$), L-ascorbic acid (L-AA), and 4-mercaptobenzoic acid (MBA) were obtained from Sigma-Aldrich (St. Louis, MO, USA) and used without further purification. The methoxy-PEG-thiol (PEG-SH, M_w = 5000) was bought from Shanghai YARE Co. Ltd. (Shanghai, China). All other chemicals were obtained from Shanghai Chemical Reagents Company (Shanghai, China). Ultrapure water was prepared using a Millipore filtration system. All glassware was soaked in aqua regia (HCl:HNO_3 in a ratio of 3:1 by volume) for 24 h and then rinsed thoroughly with ultrapure water.

Synthesis and Modification of Gold Nanoparticles (Au NPs): AuNPs with a diameter of 15 ± 2 nm were prepared by the reduction of $HAuCl_4$ with the trisodium citrate. Briefly, 1.2 mL of 1 wt% $C_6H_5Na_3O_7$ solution was quickly added to 50 mL of a boiling solution of $HAuCl_4$ (0.25×10^{-3} M) under stirring and reflux. After the color of the solution changed to deep red, the solution was refluxed for an additional 10 min. The solution was then cooled to room temperature and stored at 4 °C.

1 mL of the as-prepared AuNPs was centrifuged at 10 000 rpm for 10 min and the supernatant was removed. The AuNPs were resuspended in 0.5 mL water and the concentration was determined by UV–vis spectroscopy (≈10×10^{-9}M). 50 μL 1×10^{-3}M mPEG-SH solution

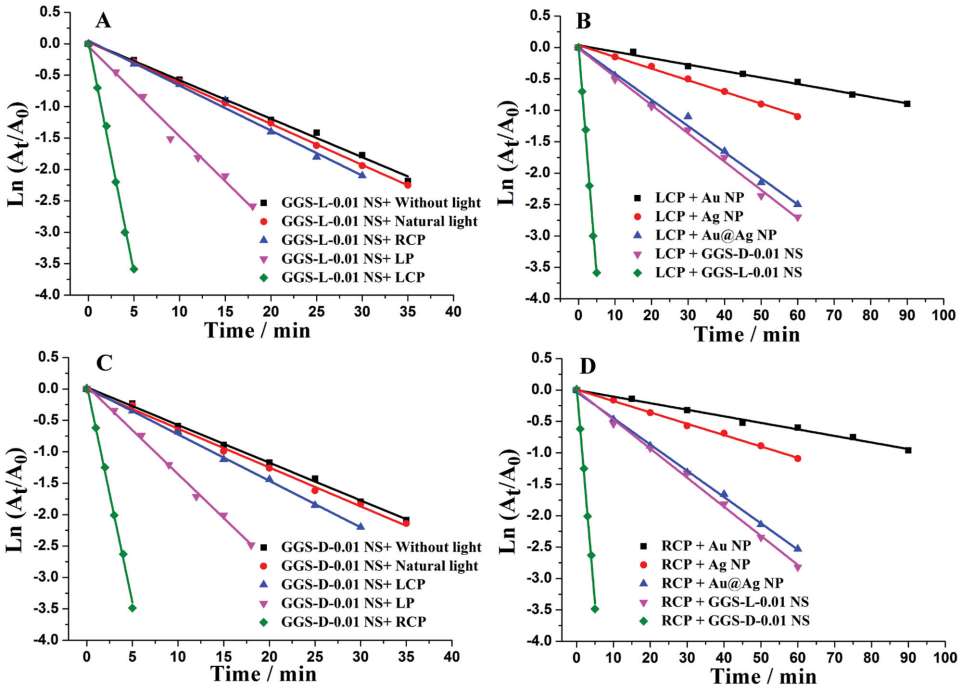

Figure 5. Photocatalytic activity evaluation of GGS NSs and the control for the reduction of 4-nitrophenol by sodium borohydride. A) Plot of Ln (A_t/A_0) as a function of time for the reaction catalyzed by GGS-L-0.01 NSs under different light conditions; B) plot of Ln (A_t/A_0) as a function of time for the reaction catalyzed by Au NPs, Ag NPs, Au@Ag NPs, GGS-D-0.01 NSs, and GGS-L-0.01 NSs under the same LCP light irradiation; C) plot of Ln (A_t/A_0) as a function of time for the reaction catalyzed by GGS-D-0.01 NSs under different light conditions; D) plot of Ln (A_t/A_0) as a function of time for the reaction catalyzed by Au NPs, Ag NPs, Au@Ag NPs, GGS-D-0.01 NSs and GGS-L-0.01 NSs under the same RCP light irradiation; A_t and A_0 are the absorption intensities at 400 nm at time t and 0, respectively.

was added to the AuNP solution. After 5 min incubation, the aqueous solution of L-cysteine at different concentrations was added. The mixture with different L-cys concentrations (0.01×10^{-3}, 0.05×10^{-3}, 0.1×10^{-3} M) was incubated at 20 °C on a shaker for 0.5 h. The solution was then centrifuged at 8000 rpm for 5 min, the supernatant was collected and the sedimentation was resuspended in 5×10^{-3} M NaCl. The AuNPs modified with different L-cys concentrations (AuNP-L-0.01, AuNP-L-0.05, AuNP-L-0.1) were then obtained. And also to prepare AuNP-D-0.01 and AuNP-D,L-0.01, 0.01×10^{-3} M D-cys and 0.01×10^{-3} M D,L-cys were used to modify AuNP, respectively.

Synthesis of Gold-Gap-Silver Nanostructures (GGS NSs): 1% PVP, 0.1 M L-AA, and 10×10^{-3} M $AgNO_3$ in ultrapure water were used for the synthesis of GGS NSs. For synthesizing GGS-L-0.01 NS, 0.5 mL AuNP-L-0.01 was mixed thoroughly with 0.1 mL 1% PVP, then 20 µL $AgNO_3$ and 20 µL L-AA were added, respectively. The resulting mixture was gently shaken at 20 °C. The reaction time was 0.5 h. The other GGS NSs were obtained using the above method. AuNP-L-0.05, AuNP-L-0.1, AuNP-D-0.01, AuNP-D-0.05, and AuNP-D,L-0.01 were used for synthesizing GGS-L-0.05 NS, GGS-L-0.1 NS, GGS-D-0.01 NS, GGS-D-0.05 NS, and GGS-D,L-0.01 NS, respectively. After the reaction, the solution was centrifuged at 5000 rpm for 6 min to remove excess reagents and redispersed in ultrapure water for further characterization.

Circularly Polarized Photocatalysis: To verify the circularly polarized photocatalytic performance of the chiral GGS NSs, three types of light were tested. The XeF laser beam (430 nm, initial power: 3 W, beam shape: 10×10 mm^2) was converted into LP (initial power: 1.5 W) light by passing it through a polarizer (10×10 mm^2, 2 nm thick). RCP (initial power: 1.5 W) light was obtained by passing the laser beam through a polarizer and a quarter-wave plate (25×25 mm^2, 1 nm thick) orientated with an angle of +45° to the plane of the incident beam. The LCP (initial power: 1.5 W) light was obtained by switching the sense of RCP by rotation of the quarter-wave plate through 90°.

A 0.1 mL aliquot of 4-nitrophenol (1×10^{-3} M) and 0.1 mL of $NaBH_4$ (0.1 M) were mixed with 1.8 mL water in a quartz cuvette. Then 30 µL of the catalyst (about 6×10^8 NPs) was added to the mixture. After that, the mixture was irradiated with different light, then the UV–vis absorption spectra of the solution were recorded immediately at a specific time interval.

Supporting Information

Supporting Information is available from the Wiley Online Library or from the author.

Acknowledgements

C.H. and L.X. contributed equally to this work. This work was financially supported by Natural Science Foundation of China (21471068, 21371081, 21301073, 21471128).

Received: June 14, 2015
Revised: July 13, 2015
Published online: August 18, 2015

[1] A. Ben-Moshe, B. M. Maoz, A. O. Govorov, G. Markovich, *Chem. Soc. Rev.* **2013**, *42*, 7028.
[2] A. Guerrero-Martínez, J. L. Alonso-Gómez, B. Auguié, M. M. Cid, L. M. Liz-Marzán, *Nano Today* **2011**, *6*, 381.

[3] J. A. Kelly, M. Giese, K. E. Shopsowitz, W. Y. Hamad, M. J. MacLachlan, *Acc. Chem. Res.* **2014**, *47*, 1088.
[4] B. Liu, Y. Cao, Z. Huang, Y. Duan, S. Che, *Adv. Mater.* **2015**, *27*, 479.
[5] C. Noguez, I. L. Garzon, *Chem. Soc. Rev.* **2009**, *38*, 757.
[6] V. K. Valev, J. J. Baumberg, C. Sibilia, T. Verbiest, *Adv. Mater.* **2013**, *25*, 2517.
[7] Y. Wang, J. Xu, Y. Wang, H. Chen, *Chem. Soc. Rev.* **2013**, *42*, 2930.
[8] Y. Zheng, L. Lin, X. Ye, F. Guo, X. Wang, *Angew. Chem. Int. Ed.* **2014**, *53*, 11926.
[9] Z. Li, Z. Zhu, W. Liu, Y. Zhou, B. Han, Y. Gao, Z. Tang, *J. Am. Chem. Soc.* **2012**, *134*, 3322.
[10] X. Wu, L. Xu, L. Liu, W. Ma, H. Yin, H. Kuang, L. Wang, C. Xu, N. A. Kotov, *J. Am. Chem. Soc.* **2013**, *135*, 18629.
[11] Y. Zhao, L. Xu, W. Ma, L. Wang, H. Kuang, C. Xu, N. A. Kotov, *Nano Lett.* **2014**, *14*, 3908.
[12] W. Ma, H. Kuang, L. Xu, L. Ding, C. Xu, L. Wang, N. A. Kotov, *Nat. Commun.* **2013**, *4*, 2689.
[13] N. Shukla, M. A. Bartel, A. J. Gellman, *J. Am. Chem. Soc.* **2010**, *132*, 8575.
[14] C. Wattanakit, Y. B. Come, V. Lapeyre, P. A. Bopp, M. Heim, S. Yadnum, S. Nokbin, C. Warakulwit, J. Limtrakul, A. Kuhn, *Nat. Commun.* **2014**, *5*, 3325.
[15] M. Yoon, R. Srirambalaji, K. Kim, *Chem. Rev.* **2012**, *112*, 1196.
[16] G. Cipparrone, A. Mazzulla, A. Pane, R. J. Hernandez, R. Bartolino, *Adv. Mater.* **2011**, *23*, 5773.
[17] A. Kuzyk, R. Schreiber, H. Zhang, A. O. Govorov, T. Liedl, N. Liu, *Nat. Mater.* **2014**, *13*, 862.
[18] A. Querejeta-Fernandez, G. Chauve, M. Methot, J. Bouchard, E. Kumacheva, *J. Am. Chem. Soc.* **2014**, *136*, 4788.
[19] J. Yeom, B. Yeom, H. Chan, K. W. Smith, S. Dominguez-Medina, J. H. Bahng, G. Zhao, W. S. Chang, S. J. Chang, A. Chuvilin, D. Melnikau, A. L. Rogach, P. Zhang, S. Link, P. Kral, N. A. Kotov, *Nat. Mater.* **2015**, *14*, 66.
[20] T. Hu, B. P. Isaacoff, J. H. Bahng, C. Hao, Y. Zhou, J. Zhu, X. Li, Z. Wang, S. Liu, C. Xu, J. S. Biteen, N. A. Kotov, *Nano Lett.* **2014**, *14*, 6799.
[21] X. Lan, Z. Chen, G. Dai, X. Lu, W. Ni, Q. Wang, *J. Am. Chem. Soc.* **2013**, *135*, 11441.
[22] X. Shen, A. Asenjo-Garcia, Q. Liu, Q. Jiang, J. Garcia de Abajo, N. Liu, B. Ding, *Nano Lett.* **2013**, *13*, 2128.
[23] C. Tan, X. Qi, Z. Liu, F. Zhao, H. Li, X. Huang, L. Shi, B. Zheng, X. Zhang, L. Xie, Z. Tang, W. Huang, H. Zhang, *J. Am. Chem. Soc.* **2015**, *137*, 1565.
[24] W. Yan, L. Xu, C. Xu, W. Ma, H. Kuang, L. Wang, N. A. Kotov, *J. Am. Chem. Soc.* **2012**, *134*, 15114.
[25] B. Yeom, H. Zhang, H. Zhang, J. I. Park, K. Kim, A. O. Govorov, N. A. Kotov, *Nano Lett.* **2013**, *13*, 5277.
[26] A. J. Mastroianni, S. A. Claridge, A. P. Alivisatos, *J. Am. Chem. Soc.* **2009**, *131*, 8455.
[27] S. H. Jung, J. Jeon, H. Kim, J. Jaworski, J. H. Jung, *J. Am. Chem. Soc.* **2014**, *136*, 6446.
[28] A. Kuzyk, R. Schreiber, Z. Fan, G. Pardatscher, E. M. Roller, A. Hogele, F. C. Simmel, A. O. Govorov, T. Liedl, *Nature* **2012**, *483*, 311.
[29] X. Lan, X. Lu, C. Shen, Y. Ke, W. Ni, Q. Wang, *J. Am. Chem. Soc.* **2015**, *137*, 457.
[30] F. Leroux, M. Gysemans, S. Bals, K. J. Batenburg, J. Snauwaert, T. Verbiest, C. Van Haesendonck, G. Van Tendeloo, *Adv. Mater.* **2010**, *22*, 2193.
[31] R. Schreiber, N. Luong, Z. Fan, A. Kuzyk, P. C. Nickels, T. Zhang, D. M. Smith, B. Yurke, W. Kuang, A. O. Govorov, T. Liedl, *Nat. Commun.* **2013**, *4*, 2948.
[32] X. Shen, C. Song, J. Wang, D. Shi, Z. Wang, N. Liu, B. Ding, *J. Am. Chem. Soc.* **2012**, *134*, 146.
[33] B. Han, Z. Zhu, Z. Li, W. Zhang, Z. Tang, *J. Am. Chem. Soc.* **2014**, *136*, 16104.
[34] L. Xu, W. Yan, W. Ma, H. Kuang, X. Wu, L. Liu, Y. Zhao, L. Wang, C. Xu, *Adv. Mater.* **2015**, *27*, 1706.
[35] I. Dolamic, S. Knoppe, A. Dass, T. Burgi, *Nat. Commun.* **2012**, *3*, 798.
[36] M. Zhu, H. Qian, X. Meng, S. Jin, Z. Wu, R. Jin, *Nano Lett.* **2011**, *11*, 3963.
[37] J. M. Slocik, A. O. Govorov, R. R. Naik, *Nano Lett.* **2011**, *11*, 701.
[38] I. Lieberman, G. Shemer, T. Fried, E. M. Kosower, G. Markovich, *Angew. Chem. Int. Ed.* **2008**, *47*, 4855.
[39] B. M. Maoz, R. van der Weegen, Z. Fan, A. O. Govorov, G. Ellestad, N. Berova, E. W. Meijer, G. Markovich, *J. Am. Chem. Soc.* **2012**, *134*, 17807.
[40] J. E. Govan, E. Jan, A. Querejeta, N. A. Kotov, Y. K. Gun'ko, *Chem. Commun.* **2010**, *46*, 6072.
[41] A. Ben Moshe, D. Szwarcman, G. Markovich, *ACS Nano* **2011**, *5*, 9034.
[42] Y. L. Zhou, M. Yang, K. Sun, Z. Y. Tang, N. A. Kotov, *J. Am. Chem. Soc.* **2010**, *132*, 6006.
[43] A. Ben-Moshe, A. O. Govorov, G. Markovich, *Angew. Chem. Int. Ed.* **2013**, *52*, 1275.
[44] A. Ben-Moshe, S. G. Wolf, M. B. Sadan, L. Houben, Z. Fan, A. O. Govorov, G. Markovich, *Nat. Commun.* **2014**, *5*, 4302.
[45] X. Wu, L. Xu, W. Ma, L. Liu, H. Kuang, W. Yan, L. Wang, C. Xu, *Adv. Funct. Mater.* **2015**, *25*, 850.
[46] D.-K. Lim, K.-S. Jeon, J.-H. Hwang, H. Kim, S. Kwon, Y. D. Suh, J.-M. Nam, *Nat. Nanotechnol.* **2011**, *6*, 452.
[47] J. W. Oh, D. K. Lim, G. H. Kim, Y. D. Suh, J. M. Nam, *J. Am. Chem. Soc.* **2014**, *136*, 14052.
[48] J. Shen, L. Xu, C. Wang, H. Pei, R. Tai, S. Song, Q. Huang, C. Fan, G. Chen, *Angew. Chem. Int. Ed.* **2014**, *53*, 8338.
[49] J. Song, B. Duan, C. Wang, J. Zhou, L. Pu, Z. Fang, P. Wang, T. T. Lim, H. Duan, *J. Am. Chem. Soc.* **2014**, *136*, 6838.
[50] X. Zhang, Z. Su, *Adv. Mater.* **2012**, *24*, 4574.
[51] K. K. Haldar, S. Kundu, A. Patra, *ACS Appl. Mater. Interfaces* **2014**, *6*, 21946.
[52] H. L. Jiang, T. Akita, T. Ishida, M. Haruta, Q. Xu, *J. Am. Chem. Soc.* **2011**, *133*, 1304.
[53] M. Avalos, R. Babiano, P. Cintas, J. L. Jimenez, J. C. Palacios, L. D. Barron, *Chem. Rev.* **1998**, *98*, 2391.
[54] N. P. Huck, W. F. Jager, B. De Lange, B. L. Feringa, *Science* **1996**, *273*, 1686.
[55] J. Kim, J. Lee, W. Y. Kim, H. Kim, S. Lee, H. C. Lee, Y. S. Lee, M. Seo, S. Y. Kim, *Nat. Commun.* **2015**, *6*, 6959.
[56] W. L. Noorduin, A. A. Bode, M. van der Meijden, H. Meekes, A. F. van Etteger, W. J. van Enckevort, P. C. Christianen, B. Kaptein, R. M. Kellogg, T. Rasing, E. Vlieg, *Nat. Chem.* **2009**, *1*, 729.
[57] Y. Wang, T. Sakamoto, T. Nakano, *Chem. Commun.* **2012**, *48*, 1871.
[58] T. Manaka, H. Kon, Y. Ohshima, G. Zou, M. Iwamoto, *Chem. Lett.* **2006**, *35*, 1028.
[59] H. Zhang, A. O. Govorov, *Phys. Rev. B.* **2013**, *87*, 075410.
[60] A. O. Govorov, Z. Fan, P. Hernandez, J. M. Slocik, R. R. Naik, *Nano Lett.* **2010**, *10*, 1374.
[61] M. L. Brongersma, N. J. Halas, P. Nordlander, *Nat. Nanotechnol.* **2015**, *10*, 25.